

**Effective Anti-Biofouling Enabled by Surface Electric Disturbance from Water Wave-
Driven Nanogenerator**

Yin Long,^{a,b} Yanhao Yu,^a Xin Yin,^a Jun Li,^a Corey Carlos,^a Xiaosong Du,^b Yadong Jiang,^b
Xudong Wang,^{a,*}

^a- Department of Materials Science and Engineering, University of Wisconsin-Madison, WI,
53706, USA

^b- State Key Laboratory of Electronic Thin Films and Integrated Devices, School of
Optoelectronic Information, University of Electronic Science and Technology of China,
Chengdu, 610054, China

*Corresponding Author : xudong.wang@wisc.edu (XW)

S1. Additional data and figures:

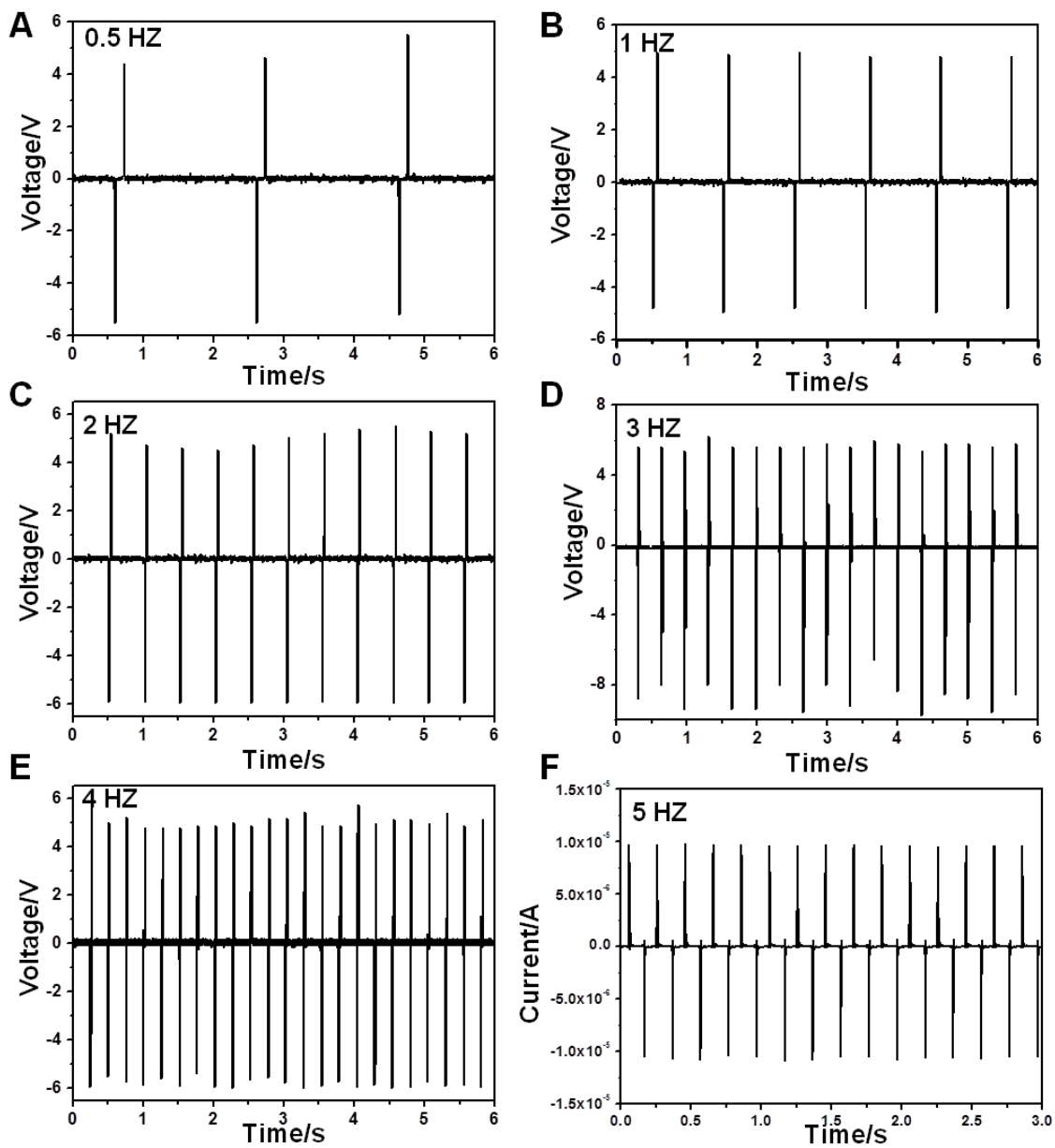


Figure S1. Electrical output of TENG. (A-E), Voltage output at frequencies from 0.5 Hz- 4 Hz. (F), Current output at 5 Hz

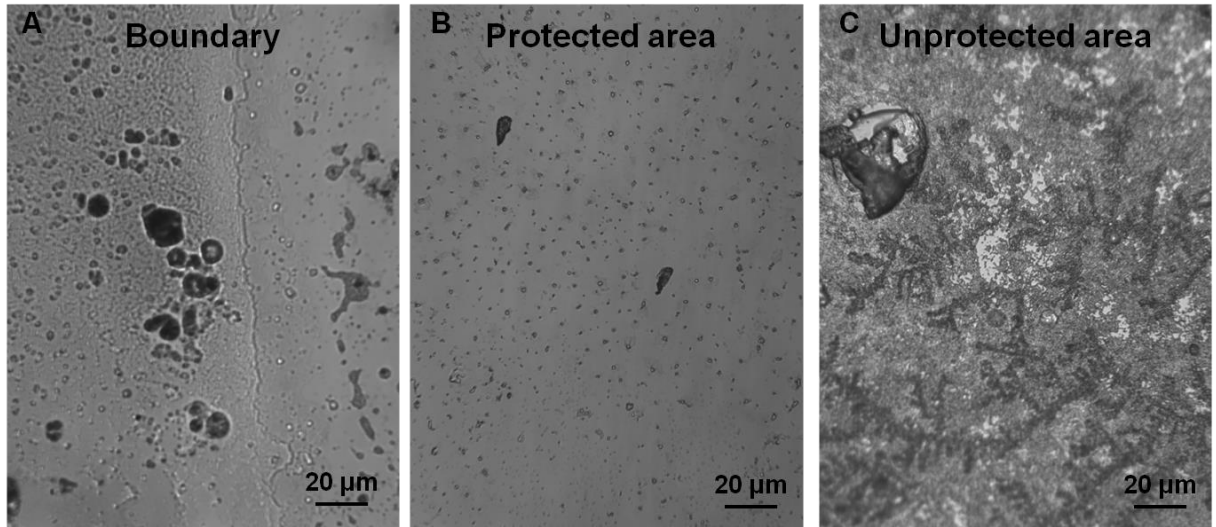


Figure. S2. Microscopic images of boundary (A), protected area (B) and unprotected area (C), The results are obtained by submerging the water wave-driven anti-biofouling glass substrate in sea water for 16 h.

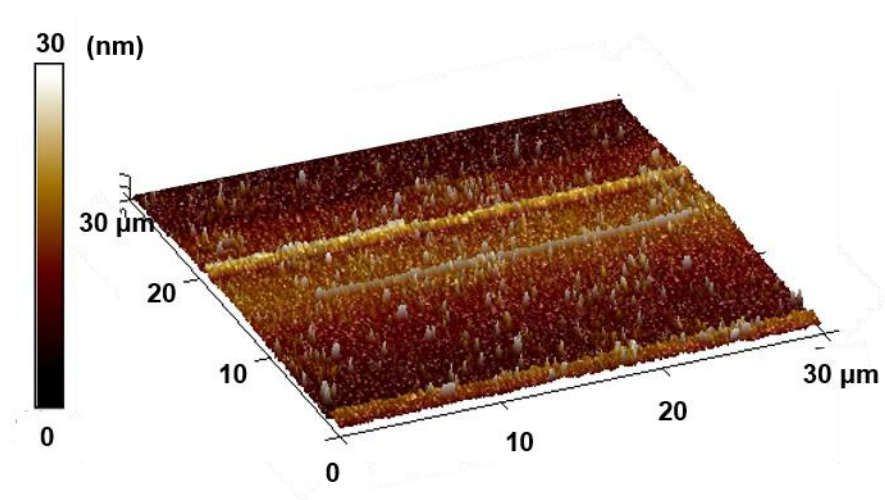


Figure. S3. AFM image of blank glass substrate.

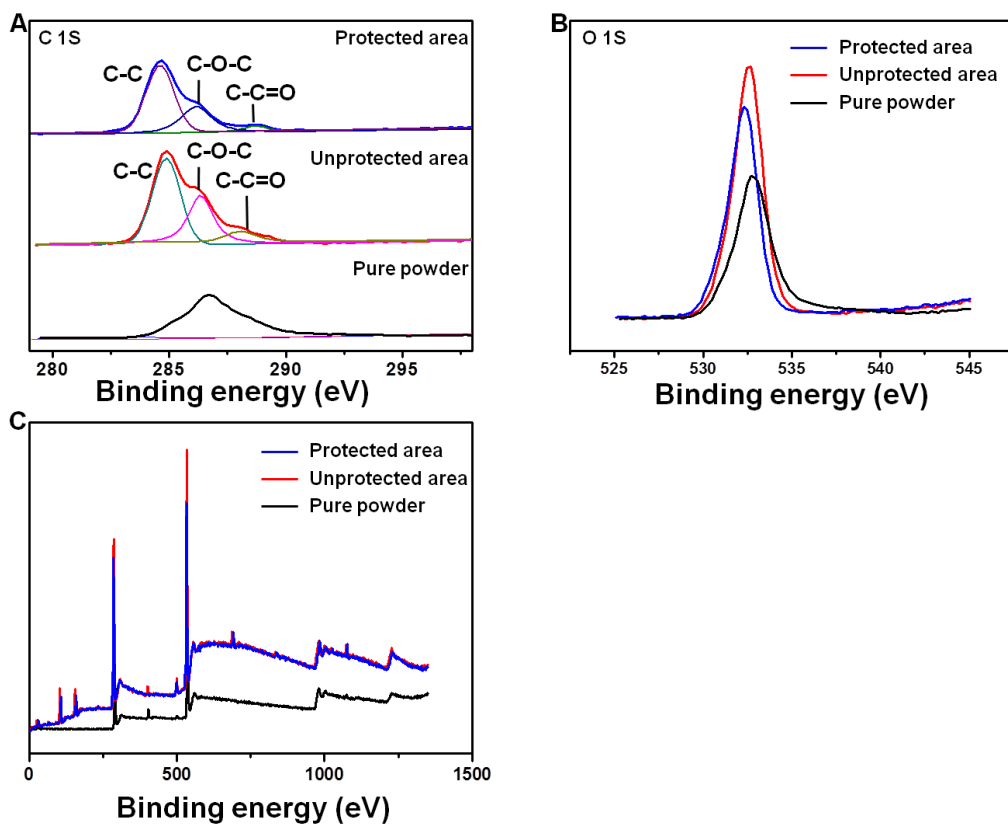


Figure. S4. XPS (A), C1s (B), O1s (C), full survey scan of pure powder, unprotected area and protected area

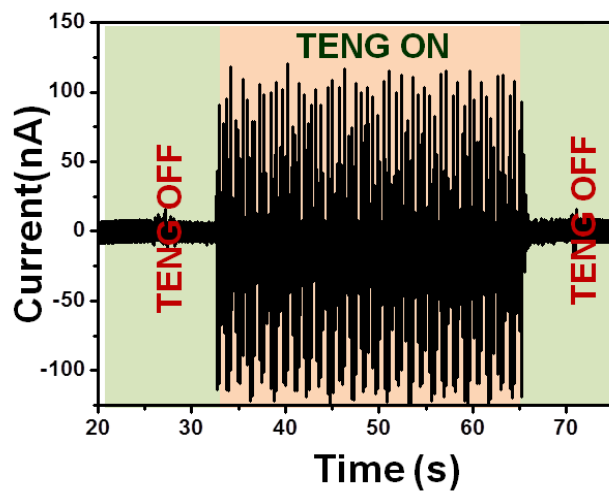


Figure. S5. Full-range current output of reference electrode (between two TENG working electrodes)

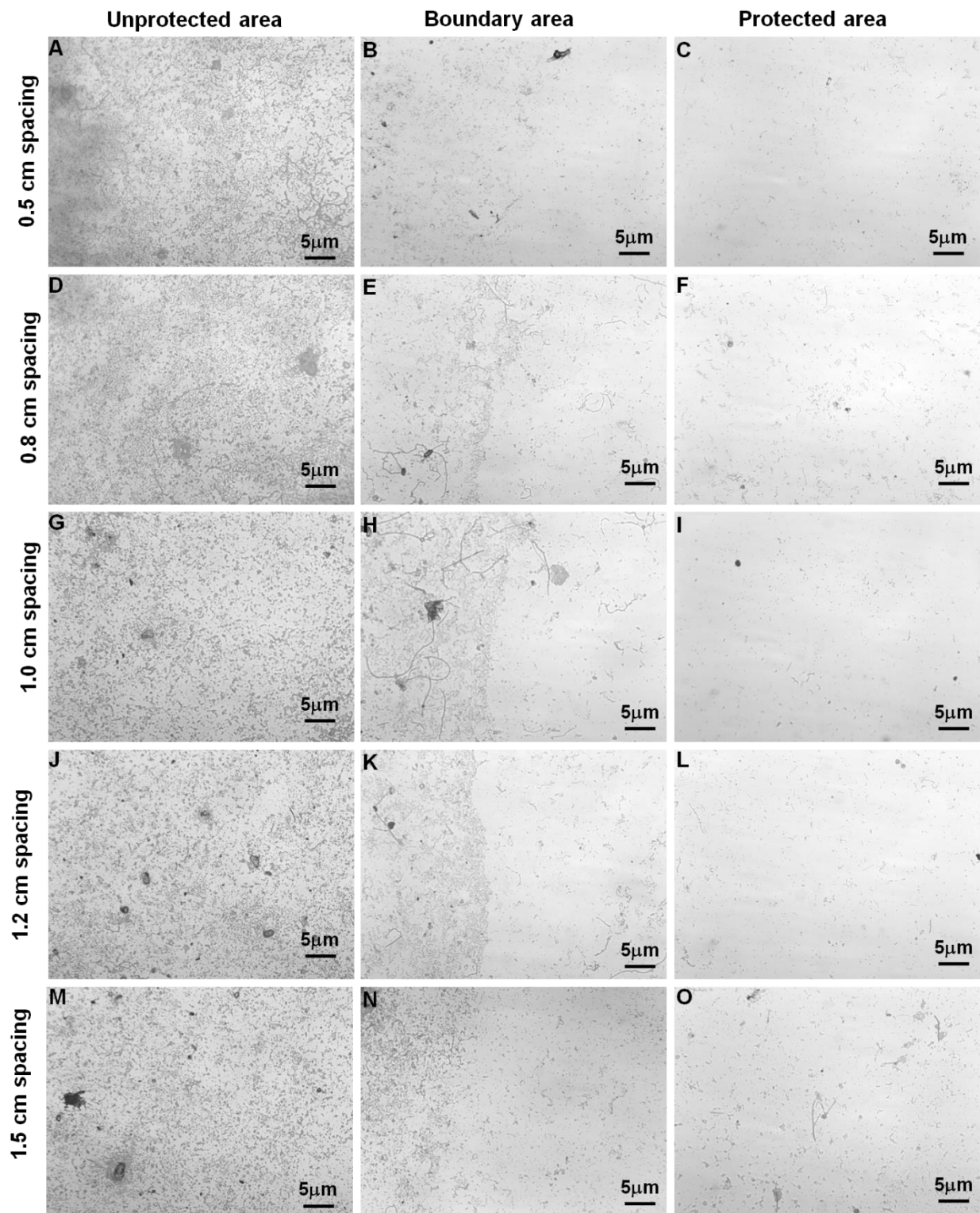


Figure. S6. Microscopic images of unprotected area, boundary and protected area with 0.5 cm (A-C), 0.8 cm (D-F), 1.0 cm (G-I), 1.2 cm (J-L), 1.5 cm (M-O) electrode spacing

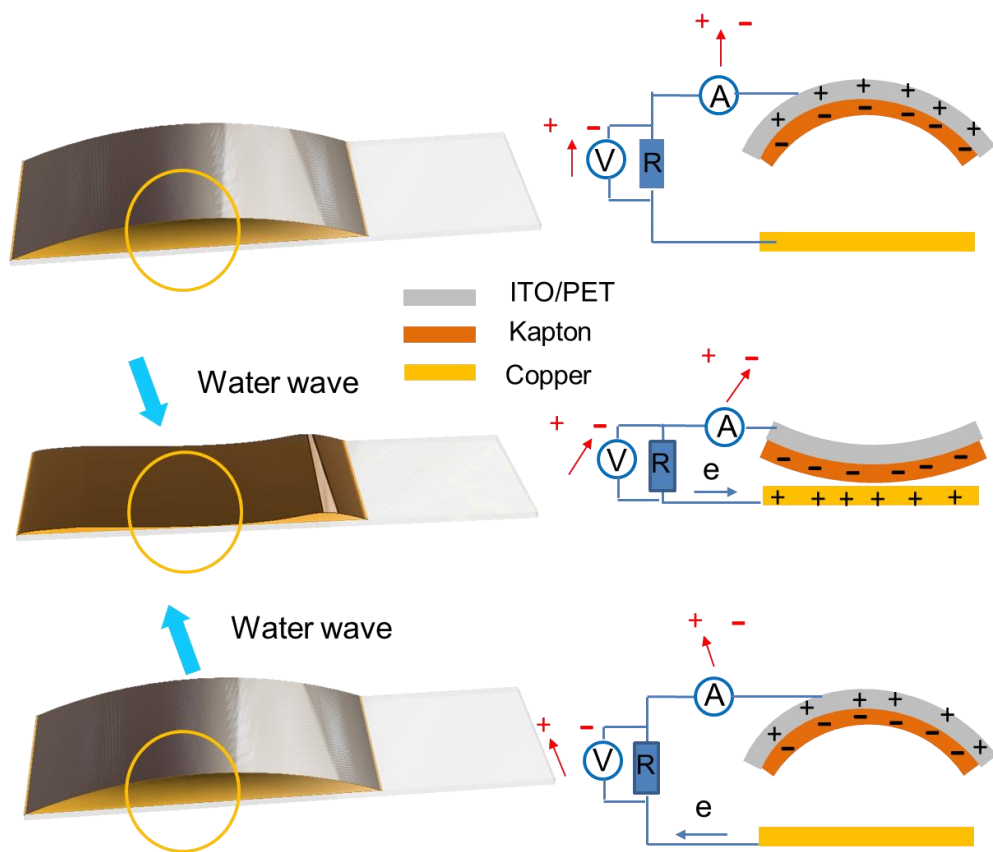


Figure. S7. The working mechanism of as-prepared water TENG.

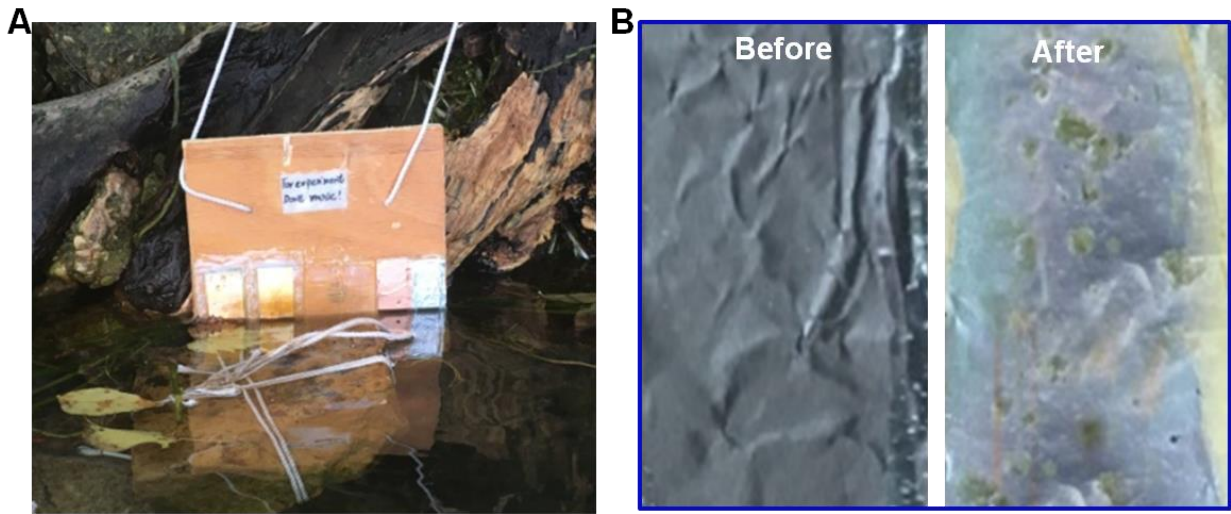


Figure. S8. Pictures of (A) experiment panel and (B) Al foil (before and after 3 weeks) in on-site experiment

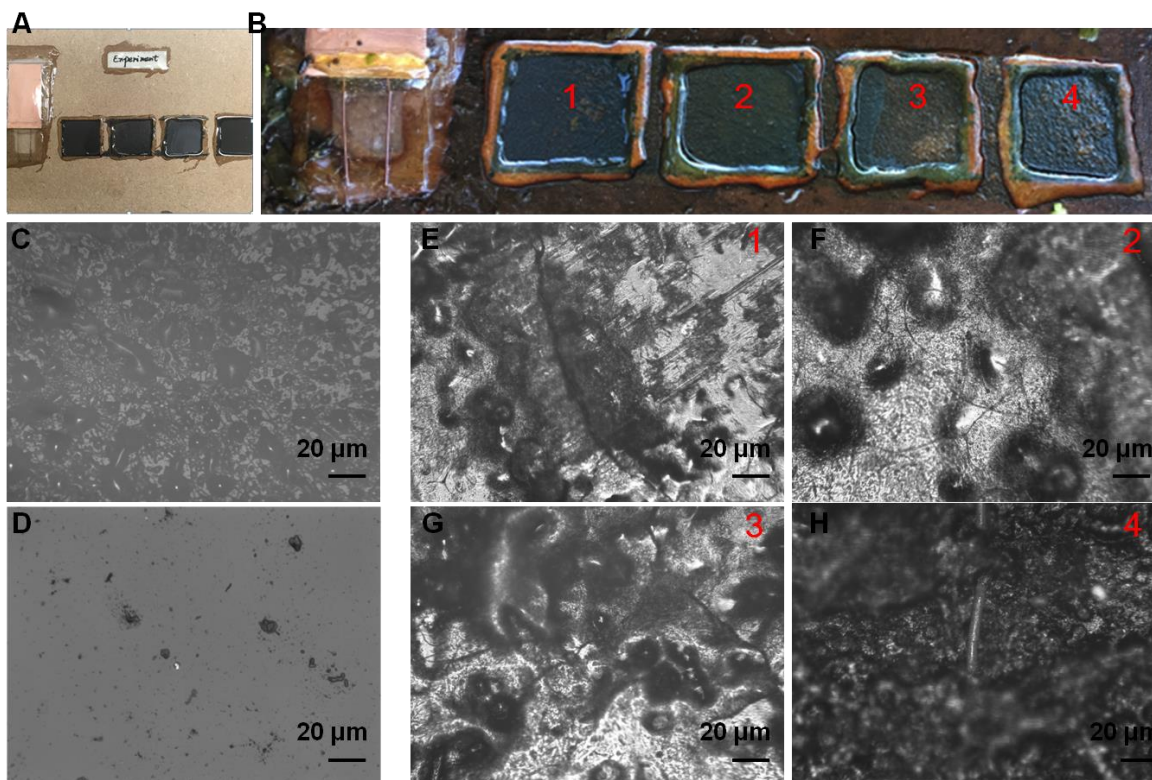


Figure. S9. Photograph of the original panel (A) and the testing panel after 4 weeks on-site testing in Lake Mendota (B). 1 to 4 were coatings of Hard hybrid ablative antifouling, Aerosol antifouling paint, Marine grade aquagard paint, and Aluminipaint, respectively. Microscopic images of unprotected area (C) and protected area (D) on the glass substrate. Microscopic images taken from the surfaces of commercial anti-fouling coatings labelled as “1” (E), “2” (F), “3” (G), and “4” (H) in (B).

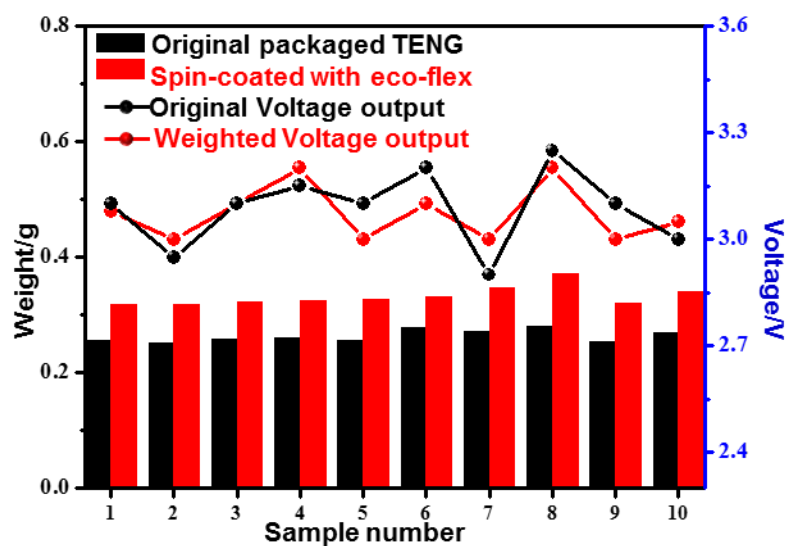


Figure. S10. Weight and voltage output of 10 original packaged TENGs and the same TENGs samples with extra spin-coated eco-flex materials. 10 packaged TENG were immersed into lake water for 7 days and the average weight increase of these devices was less than 0.01g. Therefore, a 0.08-0.09 g spin-coated Eco-flex film was equal to biofilm formed in 2 months.

S2. Anti-biofouling performance comparison:

As tributyltin (TBT) was banned by International Maritime Organization (IMO) in 2008, present anti-biofouling technology are focused on foul-release coatings (including silicone based polymers, fluoropolymer based copolymers, polymer brushes and hydrogels), photocatalysts and biomimetics. Table 1 summarizes most current representative anti-biofouling technologies and their performance in comparison to the self-activated anti-biofouling system presented in this work. This work exhibited a generally superior anti-biofouling efficiency as compared to those reported ones.

Table 1. Comparison of This Work and Other Anti-Biofouling Methods

Anti-biofouling Methods	Active Ingredient	Substrate	Test	Anti-biofouling Efficiency	Reference
Self-activated Anti-biofouling System	Electric field generated by TENG	Glass	Microorganism Reduction	85%	This work
Foul-release Coatings (Fluoropolymer Based)	Ag NPs	PVDF	Globulin Rejection	37%-16%	[1]
	Ag NPs-poly(acrylic acid)	PVDF	S. aureus and E. coli adhesion Reduction	51%-32%	[2]
	Halogenated furanone and Nafion	Glass	Biofilm Reduction	51%	[3]
	TMA-SA copolymer	PVDF	BSA Reduction	70%	[4]
	Poly(ethylene glycol) methacrylate (PEGMA)	PVDF	BSA Reduction	60%	[5]

	N-paraffin and fluorinated waxes	Glass	P. aeruginosa Reduction	42%-90%	[6]
Foul-release (Silicone Based)	PDMS-b-PMPC	Commercially available lenses	BSA Reduction	37%	[7]
Foul-release (Hydrogel Based)	Amino acids	Poly(HEMA-co-GMA) polymer	BSA Reduction	40%	[8]
Foul-release (Polymer Brush Based)	(PtBA-g Ps)-co-PPEGMEMMA	PEG	HaCaT cells Reduction	42%-81%	[9]
Foul-release (Hydrogels)	SiO2 NPs	PEG-Silicone hydrogels	BSA Reduction	40±2%	[10]
Photocatalysts	CuO and ZnO	Poly methyl methacrylate (PMMA)	Diatom Reduction	Lab:24%-38% Sea: 80%-95%	[11]
Biomimetics	Perfluorocarbon	PVC tube	Biofilm Reduction	75 %	[12]

S3. Prediction of large-scale application of TENG-driven anti-biofouling systems:

According to Ref. [13], the unit capacitance (C^0) of a pair of parallel wires can be given by:

$$C^0(pF/mm) = \frac{2\pi\epsilon}{\operatorname{ar\,cosh}\left(\frac{D^2 - 2r^2}{2r^2}\right)} \approx \frac{\pi\epsilon}{\ln\left(\frac{D}{r}\right)} \left(1 + \frac{r^2}{\ln\left(\frac{D}{r}\right)D^2}\right), D \gg r \quad (S1)$$

where ϵ is the relative permittivity, r is the radius of the wires and D is the electrode distance (Figure S6).

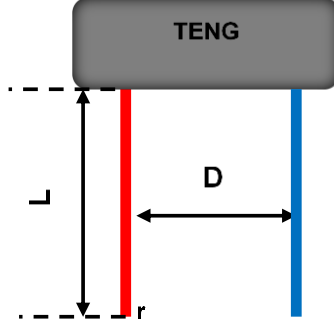


Figure. S11. Schematic showing the dimension of a TENG-driven anti-biofouling system with a simplified setup.

Thus the Capacitance (C) can be given as:

$$C = C^0 \times L \quad (\text{S2})$$

where L is the electrode length. The electric field strength can be given by $E = Q/C \times D$, where Q is the total charge. Thus E can be calculated as

$$E = \frac{Q}{C \times D} = \frac{Q}{C^0 \times L \times D} = \frac{Q}{\frac{\pi \varepsilon}{\ln\left(\frac{D}{r}\right)} \left(1 + \frac{r^2}{\ln\left(\frac{D}{r}\right) D^2}\right) \times L \times D} \quad (\text{S3})$$

In our case, the radius of electrode r is 0.0002 m, relative permittivity of glass substrate ε is 3.9, and Q is the charge generated by the TENG device. Q can be given by: $Q = \sigma \times S$, where σ is the charge density and S is the effective size (*i.e.* contact area) of TENG, $\sigma = 594.2 \mu\text{C}/\text{m}^2$ was taken from Ref. [14], thus E can be further calculated as:

$$E = \frac{594.2 \times 10^{-6} \times S}{\frac{3.9\pi}{\ln\left(\frac{D}{0.0002}\right)} \left(1 + \frac{0.0002^2}{\ln\left(\frac{D}{0.0002}\right) D^2}\right) \times 10^{-9} \times L \times D}$$

$$\begin{aligned}
&= \frac{594.2 \times 10^3 \times S}{\frac{3.9\pi}{(8.517 + \ln D) \left(1 + \frac{0.0002^2}{(8.517 + \ln D) D^2} \right)} \times 10^{-9} \times L \times D \\
&\approx \frac{594.2 \times 10^3 \times S \times (8.517 + \ln D)}{3.9\pi \times L \times D} \tag{S4}
\end{aligned}$$

Our experiments have shown that an electric field of 2 V/cm, or 200 V/m is desired to achieve effective protection to biofouling. Therefore, from equation S4, we can see that the minimum TENG size S_{min} required to reach the desired electric field as a function of the protection area is:

$$S_{min} = \frac{200 \times 3.9\pi \times L \times D}{594.2 \times 10^3 \times (8.517 + \ln D)} \tag{S5}$$

Based on Equation (S5), the S_{min} was plotted as a function of the draught depth (L) and the width of protection area (D) (Figure. S7).

As shown in Figure S7, for a yacht with a length of 6.8 m and a largest draught depth of 0.81m, the minimal TENG size required to protect the entire yacht is $S_{min} = 0.002177 \text{ m}^2$, i.e. a 5 cm \times 4.5 cm size TENG can fulfill the protection need. As for a cruise ship with a length of 184.6 m and the largest draught depth of 8.1 m, only a 75 cm \times 60 cm sized TENG would needed (Figure S8).

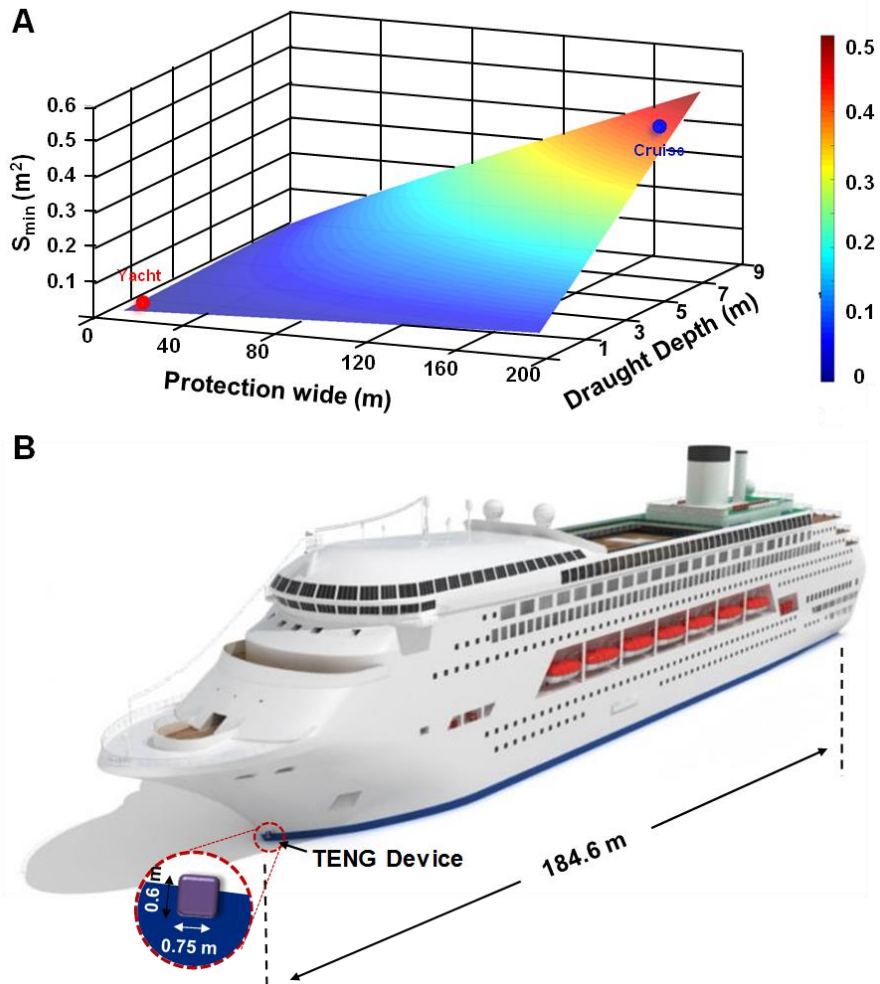


Figure. S12. (A), Minimal TENG size required to protect the under-water surface as a function of draught depth and width. The size requirements for a small yacht and a cruise ship are marked by red and blue dots, respectively. (B), Schematic illustration to compare the size of a cruise ship and the size required to protect the entire ship.

Since the protection is solely a function of the electric field and no current flow is needed, there is a lot flexibility in electrode pattern design. Although the calculation is based on one pair of electrode, in really application, electrode can be designed as interdigitated to minimize charge leakage and other environmental influences. As shown in Figure S8, electrodes can also be buried underneath of the boat paint. Thus, it won't influence any appearance of the boat but still maintain full functionality.

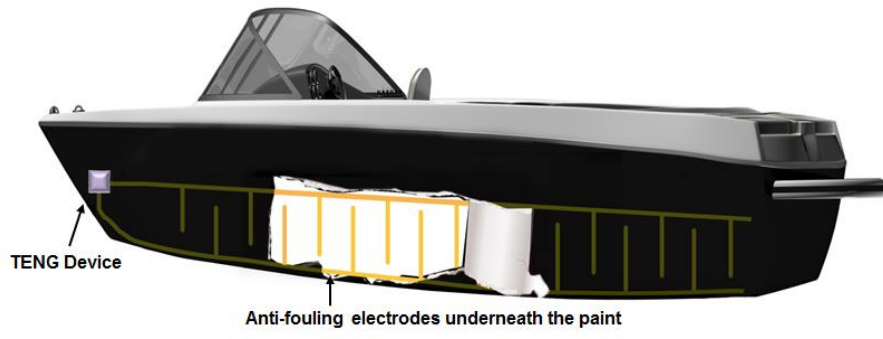


Figure. S13. Schematic showing a proposed design of electrode patterning for boat surface protection.

Large scale protection demonstration:

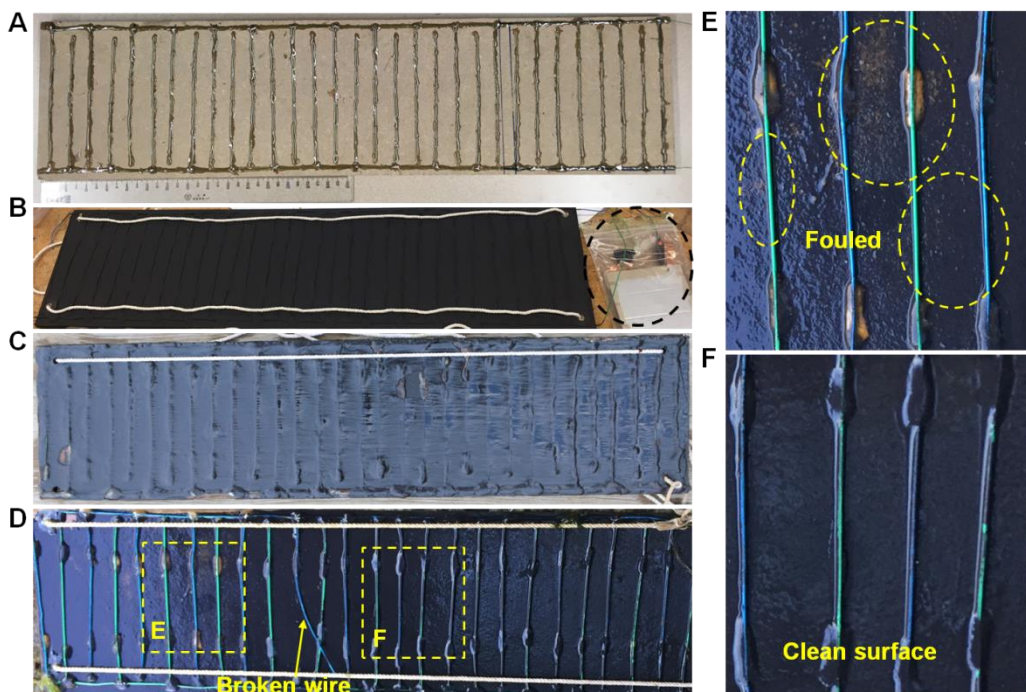


Figure. S14. Large scale anti-biofouling demonstration. (A) A fiber board covered with interdigitated electrodes for fouling protection. (B) The electrodes and board were covered by a multilayer coating of hard hybrid ablative antifouling paint to simulate the proposed boat body coating situation. (C) A clean surface after two weeks immersing the board in Lake Mendota. (D) Another board with the same anti-biofouling electrode coverage but a wire in the middle was broken on purpose to leave the left-hand side un-protective by the electric field. (E) Clear fouled areas (yellow attachments) were observed from the area without electric field. (F) The right-hand-side was still well protected showing a very clean surface.

To demonstrate the calculated large-scale anti-biofouling strategy on boat surface, we fabricated a large testing board (40" × 10") that was covered with a pair of interdigitated electrodes (Figure S12A). The board and the electrodes were then covered with multiple layers of hard hybrid ablative antifouling paint (Figure S12B) This structure could simulate the boat side structure drawn in Figure S11. The interdigitated electrodes were connected to a TENG that was fixed along the edge and sealed by multiple waterproof plastic bags. Then the entire system was placed on the shore of Lake Mendota, where the entire board was ~80% immersed under lake water. Water

waves constantly impacted on the TENG, which could generate electric potential in between the pair of interdigitated electrodes to protect the entire board. After 2 weeks of on-site test, the board was taken out and surface was remained fairly clean without any observable attachments (Figure S12C). To further show the effective of protection, another same board was fabricated and tested on site, where the electrode wire was broken in the middle area (Figure S12D). Therefore, the left side of the board was not protected by the electric field but all the other conditions were exactly the same as the right hand side. After the same 2-week in-Lake test, the board was taken out for fouling investigation (Figure S12D). As shown in Figure S12E, the left-hand side exhibited clearly fouling effect, where yellowish depositions covered multiple spots as highlighted by the yellow circles. Nevertheless, the right-hand side, which was protected by the electric field, remained a very clean surface without any hint of fouling. This experiment provided a strong support to the excellent scalability of the self-activated anti-biofouling technology from small area lab demonstration to large area boat protection.

References

- [1] S.Y. Park, J.W. Chung, Y.K. Chae, S.-Y. Kwak, *ACS applied materials & interfaces*, 5 (2013) 10705-10714.
- [2] J.-H. Li, X.-S. Shao, Q. Zhou, M.-Z. Li, Q.-Q. Zhang, *Appl. Surf. Sci.*, 265 (2013) 663-670.
- [3] Y. Wu, X. Quan, X. Si, *Int. Biodeterior. Biodegrad.*, 99 (2015) 39-44.
- [4] A. Venault, T.-C. Wei, H.-L. Shih, C.-C. Yeh, A. Chinnathambi, S.A. Alharbi, S. Carretier, P. Aimar, J.-Y. Lai, Y. Chang, *Journal of Membrane Science*, 516 (2016) 13-25.
- [5] Y. Chang, C.-Y. Ko, Y.-J. Shih, D. Qu éner, A. Deratani, T.-C. Wei, D.-M. Wang, J.-Y. Lai, *J. Membr. Sci.*, 345 (2009) 160-169.
- [6] S. Pechook, K. Sudakov, I. Polishchuk, I. Ostrov, V. Zakin, B. Pokroy, M. Shemesh, *Journal of Materials Chemistry B*, 3 (2015) 1371-1378.
- [7] L. Xu, P. Ma, B. Yuan, Q. Chen, S. Lin, X. Chen, Z. Hua, J. Shen, *RSC Advances*, 4 (2014) 15030.
- [8] C. Xu, X. Hu, J. Wang, Y.-M. Zhang, X.-J. Liu, B.-B. Xie, C. Yao, Y. Li, X.-S. Li, *ACS applied materials & interfaces*, 7 (2015) 17337-17345.
- [9] B. Xu, C. Feng, J. Hu, P. Shi, G. Gu, L. Wang, X. Huang, *ACS applied materials & interfaces*, 8 (2016) 6685-6692.
- [10] P. Yin, G. Huang, W. Tse, Y. Bao, J. Denstedt, J. Zhang, *Journal of Materials Chemistry B*, 3 (2015) 3234-3241.
- [11] S. Sathya, P.S. Murthy, A. Das, G.G. Sankar, S. Venkatnarayanan, R. Pandian, V. Sathyaseelan, V. Pandiyan, M. Doble, V. Venugopalan, *International Biodeterioration & Biodegradation*, 114 (2016) 57-66.
- [12] D.C. Leslie, A. Waterhouse, J.B. Berthet, T.M. Valentin, A.L. Watters, A. Jain, P. Kim, B.D. Hatton, A. Nedder, K. Donovan, *Nature biotechnology*, 32 (2014) 1134-1140.
- [13] J.D. Jackson, *Electrodynamics*, Wiley Online Library 1975.

[14] G. Zhu, Z.-H. Lin, Q. Jing, P. Bai, C. Pan, Y. Yang, Y. Zhou, Z.L. Wang, *Nano Lett.*, 13 (2013) 847-853.